Rewiring-induced Chaos in Pulse-coupled Neural Networks

Takashi Kanamaru† and Kazuyuki Aihara‡,††

† Department of Innovative Mechanical Engineering,
Faculty of Global Engineering, Kogakuin University,
139 Inume, Hachioji-city, Tokyo 193-0802, Japan

‡ Institute of Industrial Science, University of Tokyo,
4-6-1 Komaba, Meguro-ku, Tokyo 153-8505, Japan

†† ERATO, JST, Japan

Neural Computation, vol.24, no.4 (2012) pp.1020-1046.

Abstract

The dependence of the dynamics of pulse-coupled neural networks on random rewiring of excitatory and inhibitory connections is examined. When both excitatory and inhibitory connections are rewired, periodic synchronization emerges with a Hopf-like bifurcation and a subsequent period-doubling bifurcation; moreover, chaotic synchronization is also observed. When only excitatory connections are rewired, periodic synchronization emerges with a saddle-node-like bifurcation, and chaotic synchronization is also observed. This result suggests that randomness in the system does not necessarily contaminate the system, and sometimes randomness even introduces rich dynamics to the system such as chaos.

1 Introduction

With respect to the variability of the network structure, the Watts-Strogatz (WS) network, which is obtained by randomly rewiring the connections of locally connected regular networks, has been attracting considerable attention (Watts & Strogatz, 1998; Strogatz, 2001). When the probability of rewirings is appropriately small, the WS network has small-world network properties, namely, a small average shortest path length and a large clustering coefficient. Such properties are often observed in social networks, Internets, gene networks as well as neural networks (Strogatz, 2001). Roles of network topology on synchronization in nonlinear oscillators were well examined (Barahona & Pecora, 2002; Hong, Choi, & Kim, 2002; Hagberg & Schult, 2008). The synchronization induced by a small number of rewiring implies that signals are transmitted effectively in networks. Small-world network properties are considered important especially in the brain where efficient signal transmission should be achieved even when the volume of axon wiring is limited to some ratio of the brain size (Buzsáki, 2006). Synchronization in a rewired network composed of neuronal models intensively studied with the leaky integrate-and-fire model (Masuda & Aihara, 2004; Netoff et al., 2004; Roxin, Riecke, & Solla, 2004), the Hodgkin-Huxley-type model (Lago-Fernández et al., 2000; Buzsáki et al., 2004; Netoff et al., 2004, Kitano & Fukai, 2007), and the phase-neuron model (Kanamaru & Aihara, 2010). Some of those studies report that rewiring of the network connections yields periodic synchronization or random synchronization. However, the values of the optimal rewiring probability depends on the model, and they are not necessarily in the small-world region.

In our previous study, we analyzed the dynamics of a network of excitatory and inhibitory neurons and examined the dependence of the degree of synchronization on the rewiring probability p of the network (Kanamaru & Aihara, 2010). When $p = 1$, the network is randomly connected and it shows synchronous firing when the values of the parameters of the network are appropriately chosen (Kanamaru & Aihara, 2008). This result is consistent with that of Brunel's study (Brunel, 2000). It was also found that there exists a transition probability p_0 at which the synchronous firing emerges, and p_0 depends on the connections strength in the network. When p_0 is in the small-world region (i.e., $0.01 < p_0 < 0.1$), the firing rate of the network was much larger than biologically plausible values. On the other hand, when p_0 is far from the small-world region, complex dynamics as well as periodic dynamics were found in the network. However, we did not examine this complex dynamics in details. In the present paper, we clarify that rewiring connections of the network can give rise to chaotic dynamics in our network.

Chaos is random motion which obeys deterministic rules. Chaotic dynamics in neural systems is observed

both in single neurons *in vitro* such as the squid giant axon (Matsumoto et al., 1984; Aihara et al., 1986) and the onchidium giant neuron (Hayashi et al., 1982) and in models of single neurons (Aihara, Matsumoto, & Ikegaya, 1984; Feudel et al. 2000; Varona et al., 2001). Chaotic dynamics was also observed in models of pulse-coupled neural networks (van Vreeswijk & Sompolinsky, 1996; Tsuda et al., 2004; Kanamaru & Sekine, 2005b; Kanamaru, 2006, 2007; Kanamaru & Aihara, 2008). Moreover, it was suggested by modeling studies that chaotic dynamics is useful in some neural computations such as escape from local minima in optimization problems and chaotic transitions among memory states in associative memory models (Aihara et al., 1990; Inoue & Nagayoshi, 1991; Nara & Davis, 1992; Tsuda, 1992; Adachi & Aihara, 1997; Uchiyama & Fujisaka, 2004; Kanamaru, 2007). Some experimental studies reported that chaos also exists in biological neural networks such as the olfactory bulb of anesthetized rabbits (Freeman, 1987), but, to our knowledge, the number of such reports is few. It would be partly because the detection of chaos in a noisy high-dimensional dynamical system is difficult. Another reason would be the lack of understanding of chaos in high-dimensional dynamical systems. Therefore, it is often difficult to judge whether irregular dynamics is chaotic or not. As for the irregularity in biological neural networks, it is shown that the firing of cortical single neurons is highly irregular, and it is discussed whether this irregularity is generated by nonlinear dynamics or stochastic mechanism (Softky & Koch, 1993; Shadlen & Newsome, 1994). Moreover, it is known that spontaneous neural population activity during slow-wave sleep, anesthesia, and quiet wakefulness fluctuates between up state and down state (MacLean et al., 2005; Hoffman et al., 2007; Poulet & Petersen, 2008). Particularly, MacLean et al. (2005) proposed that the concept of attractor, i.e., deterministic mechanism can be used to understand the convergence of the observed dynamics to the up state. It is also known that the spontaneous cortical activity in the absence of external sensory input fluctuates among cortical states, many of which correspond closely to orientation maps (Kenet et al., 2003). The mechanism of such experimental observations has not been fully understood, but the random nature of chaos based on deterministic mechanism might relate to them. Therefore, it would be important to establish the detection method of chaos and understand the mechanism of chaos for noisy high-dimensional dynamical systems like neural networks.

This paper is organized as follows. We first define a network composed of excitatory and inhibitory neurons and random rewiring of connections in section 2. In an $E\&I$-rewiring network, both excitatory and inhibitory connections are rewired whereas in an E-rewiring network, only excitatory connections are rewired. The effect of rewiring in the $E\&I$-rewiring network is examined in section 3. By rewiring the connections, both periodic synchronization and chaotic synchronization are found. When the ensemble-averaged dynamics of the system has temporal structure, we call such firing as synchronous firing. Moreover, when such temporal structure is periodic or chaotic, we call such dynamics as periodic synchronization and chaotic synchronization, respectively. It was observed that the periodic synchronization emerges with a Hopf-like bifurcation. Similar results are also found in the E-rewiring network treated in section 4, but, in this case, the periodic synchronization emerges with a saddle-node-like bifurcation. In section 5, the case without chaos is discussed. Discussions and conclusions are provided in section 6.

2 Network of excitatory and inhibitory neurons

In the present study, we analyze the chaotic dynamics of the networks composed of excitatory and inhibitory neurons defined by Kanamaru & Aihara (2010). In this section, we give a brief explanation of the network. For the detailed definition, please see Appendix A.

A pulse-coupled neural network composed of excitatory and inhibitory neurons are arranged in a two-dimensional array. An excitatory neuron and an inhibitory neuron are placed at the lattice points (i, j) $(1 \leq i \leq N_x,\ 1 \leq j \leq N_y)$ in the array, and both the number of neurons in the excitatory ensemble and that in the inhibitory ensemble are $N_x N_y$. We set the values of the parameters so that the resting potentials of all the neurons are stable, i.e., they do not emit spikes without inputs. In order to generate spikes, we inject Gaussian white noise with the intensity D to each neuron. In the following, E and I denote the excitatory and inhibitory ensembles, respectively. There are four types of chemical synapses, namely, $E \leftarrow E$, $I \leftarrow E$, $E \leftarrow I$, and $I \leftarrow I$, and we set the strength of $E \leftarrow E$ and $I \leftarrow I$ synapses as g_{int}, and the strength of $I \leftarrow E$ and $E \leftarrow I$ as g_{ext}. Moreover, we introduce electrical synapses with gap junctions between inhibitory neurons ($I \leftarrow I$) based on the physiological observations (Galarreta & Hestrin, 2001), and we set its strength as g_{gap}. Recently, the existence of axo-axonal gap junctions between excitatory neurons is discussed (Traub et al., 1999; Munro & Börgers, 2010), but we have not introduced this effect in the present study.

In the limit of $N_E, N_I \to \infty$ where $N_E = N_I = N_x N_y$, this model with random connections, or the network with the rewiring probability $p = 1$ can be analyzed with the Fokker-Plank equation (Kanamaru & Sekine, 2005b; Kanamaru, 2006, 2007; Kanamaru & Aihara, 2008). By analyzing the Fokker-Plank equation using the Fourier expansion, we found various bifurcations that generate synchronous firing in the network (Kanamaru & Aihara, 2008). In the present paper, we analyze the dynamics of the network with $p \leq 1$.

Let us consider neurons in the ensemble Y which give connections by chemical synapses to a neuron at (i, j)

in the ensemble X, where $X, Y = E$ or I. $A_{cXY}^{(i,j)}$ is defined as a set of indices of such neurons. $\#A_{cXY}^{(i,j)}$ is the number of elements of this set. For simplicity, we use the symmetric connections, namely, if $(s,t) \in A_{cXY}^{(i,j)}$, then $(i,j) \in A_{cYX}^{(s,t)}$ holds. Similarly, $A_g^{(i,j)}$ denotes the set of indices of inhibitory neurons which give electrical synapses to the inhibitory neuron at (i,j). The sets of indices for connections $A_{cXY}^{(i,j)}$ and $A_g^{(i,j)}$ are defined as follows. First, we define a set $A^{(i,j)}(p,k)$, where p is the probability of the rewiring of connections and k scales the connection length. For $p = 0$, $A^{(i,j)}(0,k)$ is defined as a set of indices for local connections, namely,

$$A^{(i,j)}(0,k) = \left\{ (m,n) \,\middle|\, 1 \le d(i,j,m,n) \le \frac{k}{2} \right\} \quad (2.1)$$

$$d(i,j,m,n) = |i-m| + |j-n|, \quad (2.2)$$

where connections in both directions exist between two neurons at (i,j) and (m,n), and a periodic boundary condition is applied. The L^1 norm instead of the L^2 norm is used for simplicity. We think the usage of the L^2 norm would not affect the following results because the definition of $d(i,j,m,n)$ is used only for the network with local connections ($p = 0$), and its effect will decrease with the increase of rewired connections. The number of elements can be calculated as $\#A^{(i,j)}(0,k) = k(k+2)/2$. By rewiring the connections of $A^{(i,j)}(0,k)$ with the probability p, $A^{(i,j)}(p,k)$ is obtained. The algorithm to obtain $A^{(i,j)}(p,k)$ is explained in Appendix B. $A^{(i,j)}(p,k)$ is fixed during each simulation. The connections through the electrical synapses are always considered to be local, namely, $A_g^{(i,j)} = A^{(i,j)}(0,k)$. The rewiring is first introduced to the connections by the chemical synapses from the excitatory neurons, namely, $A_{cXE}^{(i,j)} = A^{(i,j)}(p,k)$ $(X = E, I)$. Generally, the connections from the inhibitory neurons are considered to be local, but recently, a possible role for inhibitory neurons with long-range connections is explored (Buzsáki et al., 2004). Therefore, this research considers two networks, namely, the $E\&I$-rewiring network in which the rewiring is also introduced to the connections by the chemical synapses from the inhibitory neurons as

$$A_{cXI}^{(i,j)} = A^{(i,j)}(p,k) \;\; (X = E, I), \quad (2.3)$$

and the E-rewiring network in which the connections by the chemical synapses from the inhibitory neurons are local as

$$A_{cXI}^{(i,j)} = A^{(i,j)}(0,k) \;\; (X = E, I). \quad (2.4)$$

In the following, a network with $N_x = N_y = 100$ and $k = 14$ is used. In our previous study, the dependence of synchronization on g_{ext} was analyzed in the global network that corresponds to our model with $p = 1$ and it was found that the synchronous firing exists only in certain ranges of g_{ext} (Kanamaru & Aihara, 2008). It was also found that periodic synchronous firing appears in the rewired network with $p \le 1$ (Kanamaru & Aihara, 2010). This network is sparse because the number of connections to the neuron at (i,j) is calculated to be $\#A^{(i,j)}(0,14) = 112$.

In the literature of small-world networks, the structural property of a network is often measured by the average shortest path length $L(p)$ and the clustering coefficient $C(p)$ defined in Appendix C. Note that $C(p)$ takes large values when the probability that three neurons are interconnected is large. In this network, $L(p)$ and $C(p)$ can be numerically calculated to be $L(p)/L(0) \sim 0.4$ and $C(p)/C(0) > 0.7$ in the range $0.01 \le p \le 0.1$; therefore, the network exhibits small-world properties, namely, small $L(p)$ and large $C(p)$ (Watts & Strogatz, 1998; Strogatz, 2001) in this range. $L(p)$ and $C(p)$ monotonically decrease with the increase of p similarly to those of WS model. In our previous study, we found that the synchronous firing emerges at a transition probability p_0, and the value of p_0 depends on the connections strength of the network (Kanamaru & Aihara, 2010). When p_0 is in the small-world network region, the firing rate of the network becomes much larger than biologically plausible values. When p_0 is far from the small-world network region, chaos-like dynamics as well as periodic dynamics were also found in the network. In the following, we focus on the chaos-like dynamics observed in our network.

3 Effect of rewiring on synchronization in the $E\&I$-rewiring network

In the following, the parameters are set to $g_{gap} = 0.10$, $g_{int} = 5$, $g_{ext} = 3.3$, and $D = 0.004$ so that this network shows synchronous firing for $p = 1$ (Kanamaru & Aihara, 2008). Figure 1 shows the firing of neurons in the $E\&I$-rewiring network with $p = 0.3$ and $p = 0.8$. The firing for $p = 0.3$ in Figures 1B and 1D shows that there is little correlation in the firing of neurons. Note that the firing of each neuron is stochastic because this firing is induced by noise $\xi_X^{(i,j)}(t)$. The firing rates J_E and J_I of the excitatory and inhibitory ensemble are defined as an average instantaneous firing rate of neurons, namely,

$$J_X(t) \equiv \frac{1}{N_x N_y w} \sum_{(i,j)} \sum_l \Theta(t - t_l^{(i,j)}), \quad (3.1)$$

$$\Theta(t) = \begin{cases} 1 & \text{for } 0 \le t < w \\ 0 & \text{otherwise} \end{cases}, \quad (3.2)$$

where $t_l^{(m,n)}$ denotes the lth firing time of the neuron at (m,n) in the ensemble Y and is defined by the time at which $\theta_Y^{(m,n)}$ exceeds π, and $w = 1$. In the following, we apply a low-pass filter with the cutoff frequency $f_c = \frac{1}{2\pi}$ to J_E and J_I twice in order to obtain smooth functions before observation. J_E and J_I for $p = 0.3$ are shown in Figures 1A and 1C, respectively, and fluctuation around each equilibrium is observed. This fluctuation means that there is little correlation among the firing times of

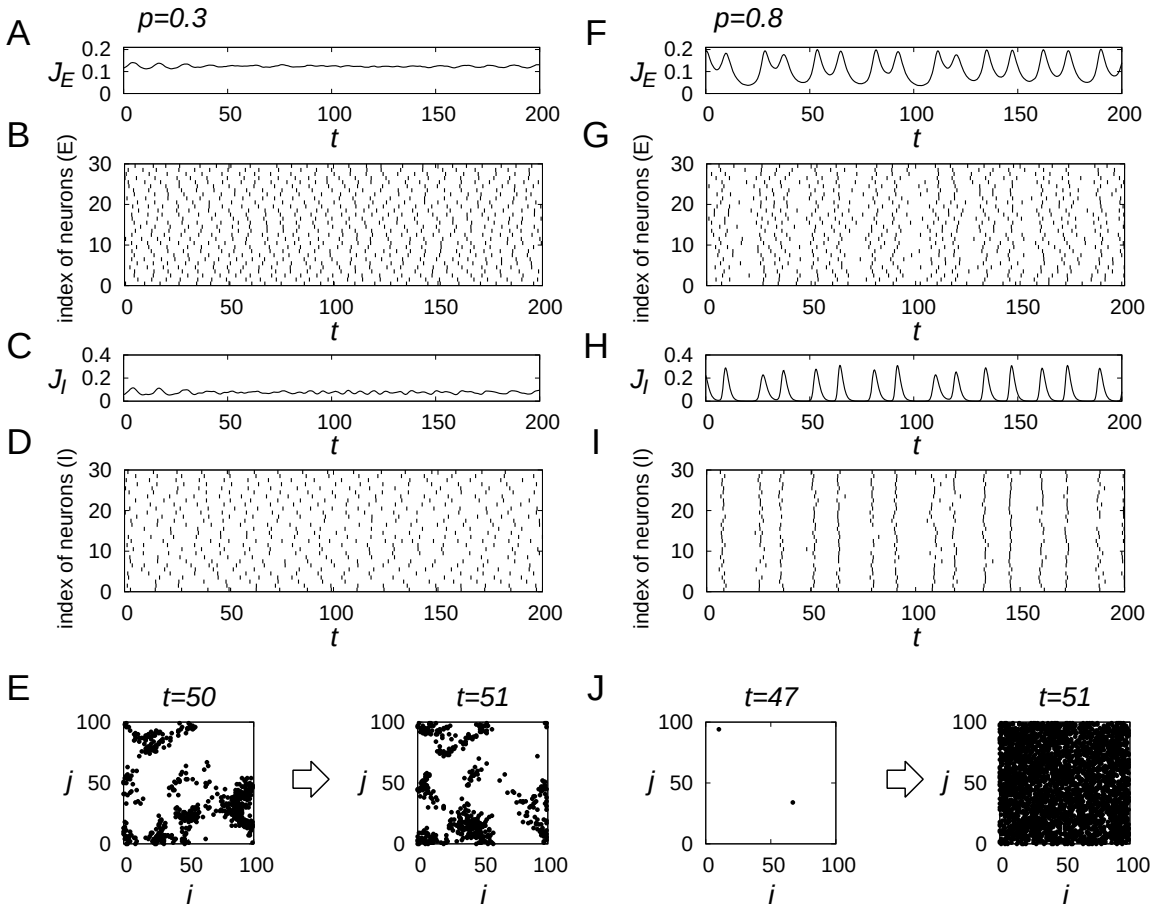

Figure 1: The firing of neurons in the $E\&I$-rewiring network for $p = 0.3$ ((A)-(E)) and $p = 0.8$ ((F)-(J)) with $N_x = N_y = 100$, $k = 14$, $g_{gap} = 0.10$, $g_{int} = 5$, $g_{ext} = 3.3$, and $D = 0.004$. (A), (C), (F), (H) Temporal changes in the firing rates J_E and J_I of the excitatory and inhibitory ensemble. (B), (D), (G), (I) Corresponding raster plots of the firing of neurons. The firing of 30 neurons among 10000 neurons in each ensemble is shown. The index of the neuron at (i, j) is calculated as $jN_x + i$. (E), (J) The spatial firing pattern of neurons in the two-dimensional array. The positions of inhibitory neurons which fire within a time window of width 0.5 are plotted. The firing of the inhibitory neurons is shown because the spatial contrast is clearer than that of the excitatory neurons.

neurons. In Figure 1E, the spatial firing pattern of the neurons in the two-dimensional array is shown. It is observed that the clusters of firing appear stochastically.

On the other hand, as shown in Figures 1G and 1I, there are some correlations in the stochastic firing of neurons, and the ensemble-averaged values of J_E and J_I temporally and coherently changes. We refer to such firing as synchronous firing in the following. Moreover, when such temporal structure is periodic or chaotic, we call such dynamics as periodic synchronization and chaotic synchronization, respectively. To clarify how synchronous firing emerges, the dependence of J_E peaks on p is plotted in Figure 2C. For $p < 0.4$, the peaks of J_E keep small values because the dynamics of the network fluctuates around an equilibrium on the $(J_E,\ J_I)$ plane as shown in Figure 2A. Such dynamics corresponds to asynchronous firing of neurons. On the other hand, for $p > 0.4$, the peaks of J_E become larger, and the dynamics of J_E has developed structure shown in Figure 2B. Moreover, this structure would be chaotic as shown below.

Figures 3A and 3B show the power spectra $P(f)$ of J_E with several peaks for $p = 0.6$ and 0.8, respectively. As p increases from small values, a peak height of $P(f)$ starts to increase at a critical p; we call the frequency of this peak f_1. Then $f_{1/2}$ is defined as the frequency which takes a peak of $P(f)$ around $f_1/2$. In this case, $f_1 \simeq 0.07$ and $f_{1/2} \simeq 0.035$. $P(f)$ has very sharp peaks like δ function for periodic synchronization as shown in Figure 3A, but, when chaos-like dynamics exists in the system, it has somewhat broader peaks as shown in Figure 3B; therefore, we cannot directly compare the values of peaks of $P(f)$ for different p in order to quantify the power of the peak at frequency f. For comparison, a sum of

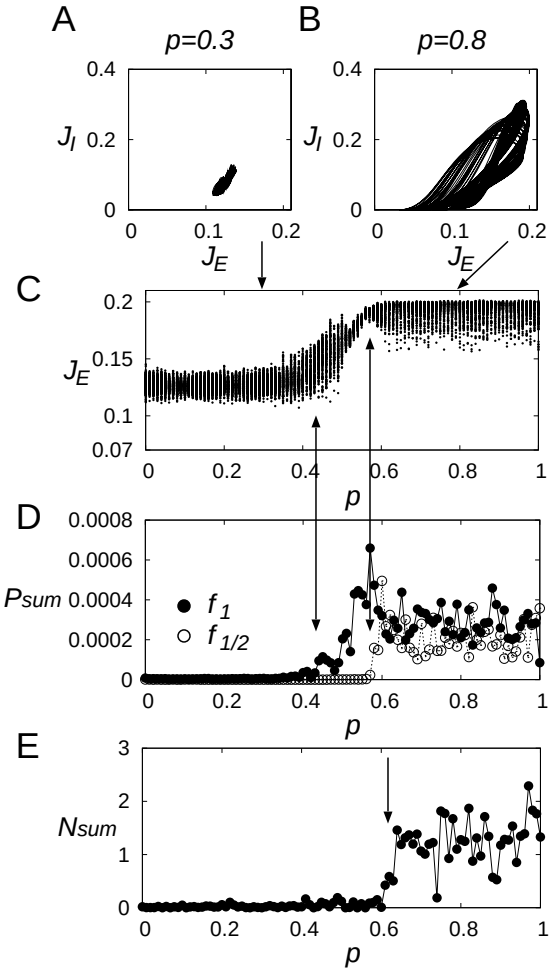

Figure 2: The dependence of the dynamics in the $E\&I$-rewiring network on the rewiring probability p for $g_{ext} = 3.3$. (A), (B) Trajectories on the (J_E, J_I) plane for $p = 0.3$ and $p = 0.8$. (C) Plot of peak values of J_E. (D) The dependence of the sum of powers around f_1 and $f_{1/2}$ on p. (E) Dependence of the sum of nonlinearity on p.

powers is defined as

$$P_{sum}(f) = \int_{f_m}^{f_M} P(f')df', \tag{3.3}$$

where $f_m < f_M$, $P(f_m) = P(f_M) = P(f)/2$ and for $\forall f' \in (f_m, f_M), P(f') > P(f)/2$. The dependence of $P_{sum}(f_1)$ and that of $P_{sum}(f_{1/2})$ on p are shown in Figure 2D. As p increases, the sum of powers at f_1 and the amplitude of J_E start to increase at $p \simeq 0.4$. In other words, after the emergence of periodic synchronization, J_E peak increases with the increase of the bifurcation parameter. This phenomenon is similar to the supercritical Hopf bifurcation. To confirm the similarity of this process to the Hopf bifurcation, we also examined the dependence of the frequency f_{max} that maximizes $P(f)$ on p. As shown in Figure 4, around $p \simeq 0.4$, f_{max} takes almost constant values ($f_{max} \simeq 0.08$), i.e., the system

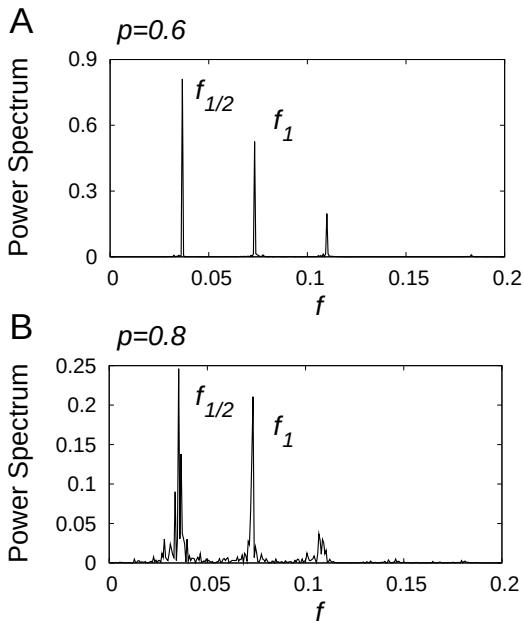

Figure 3: Power spectra $P(f)$ of J_E in the $E\&I$-rewiring network for (A) $p = 0.6$ and (B) $p = 0.8$.

has a periodic component even when a stable limit cycle does not exist (see also Figure 1A). This situation is also

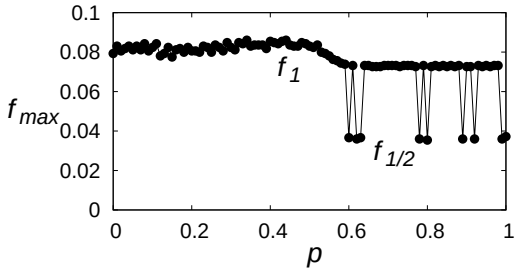

Figure 4: The dependence of the frequency f_{max} that maximizes $P(f)$ on p.

similar to the Hopf bifurcation, at which the real part of the complex conjugate eigenvalues $\lambda \pm \omega i$ ($\omega \neq 0$) at the equilibrium takes zero. We cannot conclude, however, that this bifurcation is a Hopf bifurcation because our network is governed by stochastic differential equations. Therefore, we call this bifurcation as a Hopf-like bifurcation in the following. For $p \geq 0.6$, f_{max} sometimes takes the values around 0.04, which is similar to a period-doubling bifurcation. As shown in Figure 2D, the sum of power at $f_{1/2}$ starts to increase at $p \simeq 0.58$, and this would correspond to a period-doubling bifurcation point. Successive period-doubling bifurcations might exist for larger values of p, but we could not detect it because of fluctuations in the network.

In the following, we examine whether chaotic synchronization exists in the network, using the nonlin-

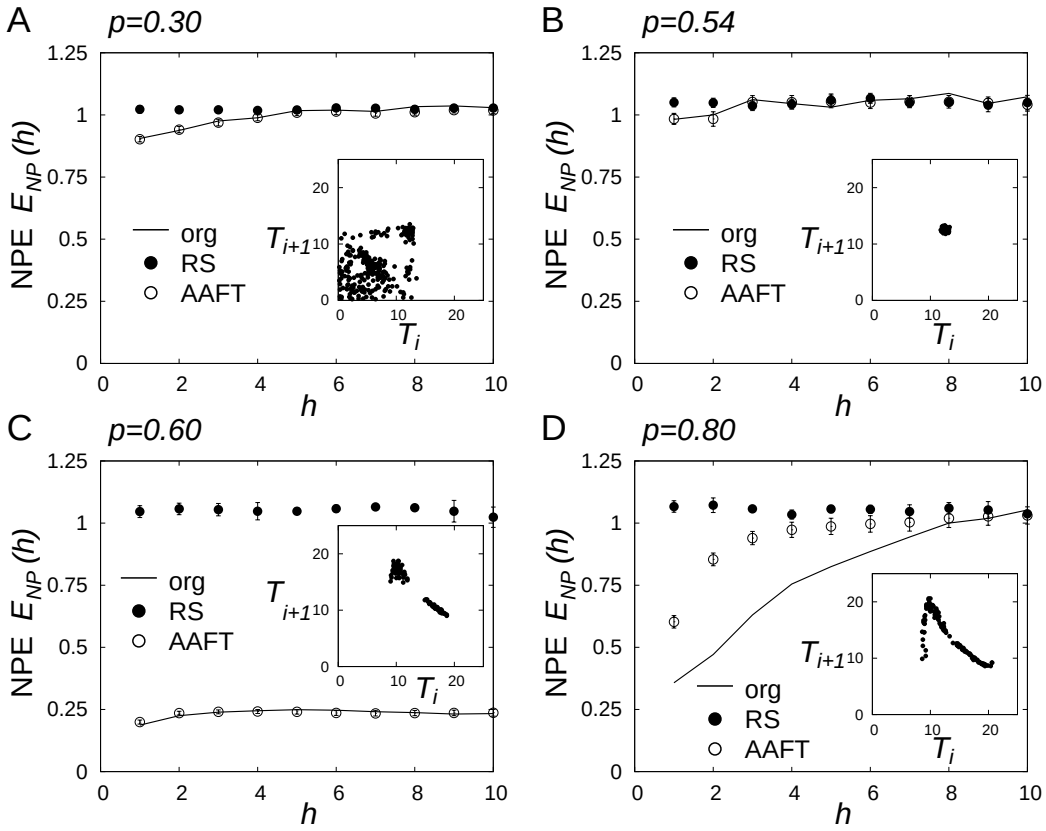

Figure 5: The dependence of the nonlinear prediction error $E_{NP}(h)$ on prediction step h for the time series of the inter-synchronization interval (ISI) data T_i, which are obtained from the $E\&I$-rewiring network with the rewiring probabilities $p = 0.3$, 0.54, 0.6, and 0.8. The results for the original time series are shown with solid lines, and mean values and the standard deviations for 100 samples of surrogate data (RS and AAFT; see Appendix D) are also shown with filled and open circles, respectively. The inset in each figure shows the return plot on the (T_i, T_{i+1}) plane.

ear prediction method based on reconstruction of the inter-synchronization interval (ISI) data T_i (Aihara & Tokuda, 2002), which is summarized in Appendix D. In this method, we use surrogate data defined as alternate data sets generated from the original data set, which are widely used for hypothesis testing in nonlinear time series analysis (Theiler et al., 1992; Sauer, 1994; Suzuki, et al., 2000; Shinohara et al., 2002; Kanamaru & Sekine, 2005a; Hirata et al., 2008). In general, to use surrogate data for hypothesis testing, a null hypothesis is set. Based on this null hypothesis, specific characteristics of the ISI are preserved, while others are randomized to generate surrogates. In the following analysis, we use the random shuffled (RS) surrogate data and the amplitude adjusted Fourier transformed (AAFT) surrogate data, which correspond to the null hypothesis that the observed ISIs are independent and identically distributed random process and that of a linear stochastic process observed through a monotonic nonlinear function, respectively. The nonlinear prediction error $E_{NP}(h)$ for the prediction step h is calculated for three data, namely, the original data, the RS surrogate data, and the AAFT surrogate data. If $E_{NP}(h)$ of the original data is significantly different from those of RS and AAFT surrogate data, the null hypothesis on independent and identically distributed random process and that on a linear stochastic process observed through a monotonic nonlinear function can be rejected for the original data, and it can be concluded that there is some possibility that the original time series has deterministic structure, such as a strange attractor. On the other hand, when there is no significant difference between the original data and the surrogate population, we do not reject the null hypotheses of this surrogate. In such a case, we characterize the dynamics of the original data based on the behavior of $E_{NP}(h)$ and return plot of T_i (see below), such as a random walk around a stable equilibrium, a noisy limit cycle whose period is stochastically fluctuating, etc. Figure 5 shows the dependence of $E_{NP}(h)$ on the prediction step h for the time series obtained from the network with the rewiring probabilities $p = 0.3$, 0.54, 0.6, and 0.8. The $E_{NP}(h)$ for the original time series are shown with solid lines, and mean values for 100 samples of surrogate data (RS and AAFT) are also shown

with filled and open circles with their standard deviations, respectively. As shown in Figure 5A, $E_{NP}(h)$ for $p = 0.3$ takes values close to 1, meaning that deterministic prediction is difficult in this time series. Moreover, for $p = 0.3$, $E_{NP}(h)$ of the original data is not significantly different from those of AAFT surrogate data; therefore, the null hypothesis cannot be rejected and this dynamics can be regarded as a linear stochastic process observed through a monotonic nonlinear function. Similarly, the result of the original data for $p = 0.54$ in Figure 5B is not significantly different from those of AAFT surrogate data; therefore, the null hypothesis cannot be rejected and this dynamics can also be regarded as such a linear stochastic process. In this case, it is observed that the return plot on the (T_i, T_{i+1}) plane fluctuates around a single point; therefore, we regard this dynamics as periodic synchronization (i.e., $T_i \simeq T_{i+1}$) whose fluctuations are regarded as a linear stochastic process. It is observed that $E_{NP}(h)$ for $p = 0.6$ shown in Figure 5C takes small values because the deterministic prediction is easy due to the existence of the periodic structure with two cycles as shown in the return plot on the (T_i, T_{i+1}) plane. Moreover, also in this case, $E_{NP}(h)$ of the original data is not significantly different from those of AAFT surrogate data. Therefore, we regard this dynamics as noisy periodic synchronization with two cycles whose fluctuations are regarded as a linear stochastic process. Note that the dynamics is generated by the period-doubling bifurcation at $p \simeq 0.58$ (see Figure 2D). $E_{NP}(h)$ for $p = 0.8$ shown in Figure 5D also takes small values, but is significantly different from those of RS and AAFT surrogate data. Therefore, the null hypothesis on a linear stochastic process observed through a monotonic nonlinear function can be rejected for this time series with $p = 0.8$, and it can be concluded that there is some possibility that the original time series has deterministic structure. It should be noted that $E_{NP}(h)$ increases with the increase of the prediction step h in Figure 5D. In other words, the information about initial conditions is rapidly lost. Moreover, the return plot on the (T_i, T_{i+1}) plane approximately shows a one-dimensional unimodal structure. From these observations, we conclude that the network rewired with $p = 0.8$ shows chaotic synchronization.

To judge whether the time series has chaotic properties, we define the sum of nonlinearity N_{sum} as

$$N_{sum} = \sum_{h=1}^{10} \Theta(E_{NP}^{AAFT}(h) - \sigma^{AAFT}(h) - E_{NP}(h)), \tag{3.4}$$

$$\Theta(x) = \begin{cases} x & (x \geq 0) \\ 0 & (x < 0) \end{cases}, \tag{3.5}$$

where $E_{NP}^{AAFT}(h)$ and $\sigma^{AAFT}(h)$ are the mean nonlinear prediction error and standard deviation of AAFT surrogate data, respectively. Note that large N_{sum} implies that the existence of nonlinear deterministic structure because $E_{NP}(h)$ is significantly different from that of AAFT surrogate data. The dependence of N_{sum} on the rewiring probability p is shown in Figure 2E. N_{sum} takes large values for $p > 0.6$, and there is some possibility that the network shows chaotic synchronization in this range.

4 Effect of rewiring on synchronization in the E-rewiring network

In the previous section, the effect of rewiring the $E\&I$-rewiring network was examined. Although inhibitory neurons also have long-range connections in neural systems (Buzsáki et al., 2004), it is often thought that the long-range connections are mainly excitatory. Therefore, we examine herewith the effect of rewiring on synchronization in the E-rewiring network. Similarly to the

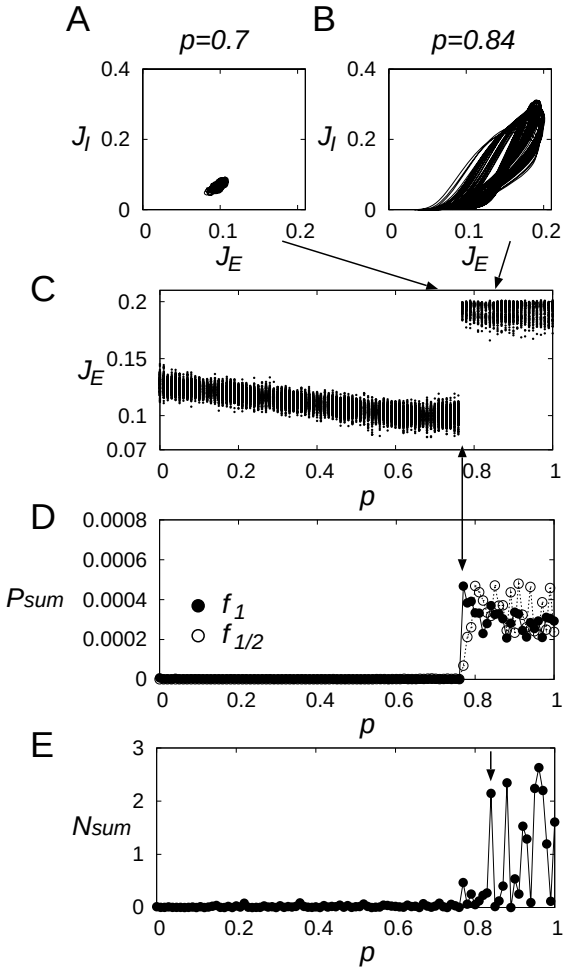

Figure 6: The dependence of the dynamics in the E-rewiring network on the rewiring probability p for $g_{ext} = 3.3$. (A), (B) Trajectories on the (J_E, J_I) plane for $p = 0.7$ and $p = 0.84$. (C) Plot of peak values of J_E. (D) The dependence of the sum of powers around f_1 and $f_{1/2}$ on p. (E) Dependence of the sum of nonlinearity on p.

$E\&I$-rewiring network (Figure 2), periodic synchronization emerges at $p \simeq 0.78$ and chaotic synchronization emerges at $p \simeq 0.84$ in the E-rewiring network as shown in Figure 6. The transition probability p of rewiring is larger than that in the $E\&I$-rewiring network because the rewiring number in the E-rewiring network is smaller. Moreover, the transition to periodic synchronization takes place abruptly at $p_0 = 0.7639$ as shown in Figure 6C, and this suggests that the bifurcation that yields periodic synchronization is different from that of $E\&I$-rewiring network. We further investigate this bifurcation.

For $p < p_0$, J_E converges to a stationary value after spending a transient time interval T_c with the periodic behavior as shown in Figure 7. Note that we set the

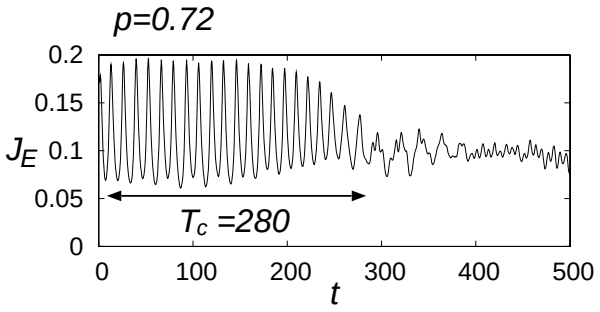

Figure 7: A temporal change of J_E for $p = 0.72$ in the E-rewiring network. J_E converges to a stationary value after spending a transient time interval T_c with the periodic behavior.

initial phases of all the neurons randomly in the range $[0, 2\pi]$. Some neurons whose internal states are close to but less than the threshold π would fire immediately after the start of our simulation. Then the network shows transient synchronization during the time interval T_c. We call T_c the converging time in the following discussion. Such an evolution is often observed when the periodic solution is generated by a saddle-node bifurcation of a stable limit cycle and an unstable limit cycle (Ott, 1993). The dependence of the averaged converging time $\langle T_c \rangle$ over 10 samples on p is shown in Figure 8. The relationship

$$\langle T_c \rangle \propto (p_0 - p)^{-1/2} \tag{4.1}$$

is observed which is typical to the saddle-node bifurcation (Ott, 1993); therefore, the transition to periodic synchronization would be realized by the saddle-node bifurcation.

For $p > p_0$, chaotic synchronization is also observed in the E-rewiring network (see Figure 6E) although its range is narrower than that of the $E\&I$-rewiring network.

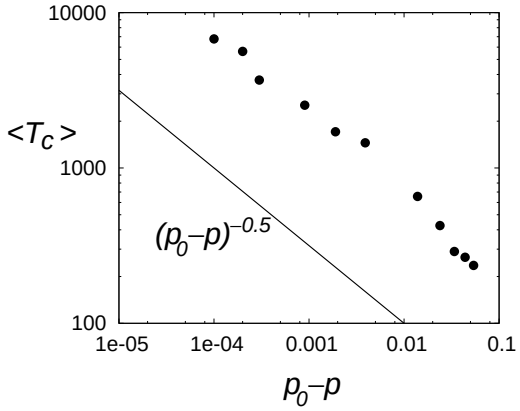

Figure 8: The dependence of the averaged converging time $\langle T_c \rangle$ on the rewiring probability p. The average was calculated over 10 samples.

5 Transition without chaos

In sections 3 and 4, the connection strength between excitatory and inhibitory ensembles is set to $g_{ext} = 3.3$, and we observed the rewiring-induced chaotic synchronization both in the $E\&I$-rewiring network and in the E-rewiring network. Similarly, there are transitions to the synchronized state without chaos depending on the values of the parameters of the network.

In this section, we set $g_{ext} = 3.2$, which is the value mainly used in our previous study (Kanamaru & Aihara, 2010), and we observe the dynamics of the network. Figures 9 and 10 show the dependence of the dynamics on the rewiring probability p in the $E\&I$-rewiring network and that in the E-rewiring network, respectively.

In each network, the power spectrum does not have a peak at $f_{1/2}$ as shown in Figures 9D and 10D; therefore, the period-doubling bifurcation does not take place when $g_{ext} = 3.2$ in these networks. Moreover, the sum of nonlinearity fluctuates around zero as shown in Figures 9E and 10E; therefore, chaotic dynamics is not observed in the time series obtained from these network.

The reason for this difference of the dynamics is because chaos in our network depends on both p and g_{ext}. Figure 11 shows the dependence of the chaotic structure on p and g_{ext}. Each inset shows the return plot (T_i, T_{i+1}) of the ISI (see also Figure 5). It is observed that chaos (or unimodal structure) exists when both p and g_{ext} are large. When p becomes large, the ISI T_i tends to become long (data not shown). On the other hand, when g_{ext} becomes large, the ISI T_i tends to become short. Therefore, for large p and g_{ext}, a competition for the length of ISI takes place, then the period-doubling and generation of chaos will take place.

In summary, we found both the rewiring-induced chaotic synchronization (Sections 3 and 4) and the rewiring-induced periodic synchronization (Section 5). Those dynamical properties of the network are deter-

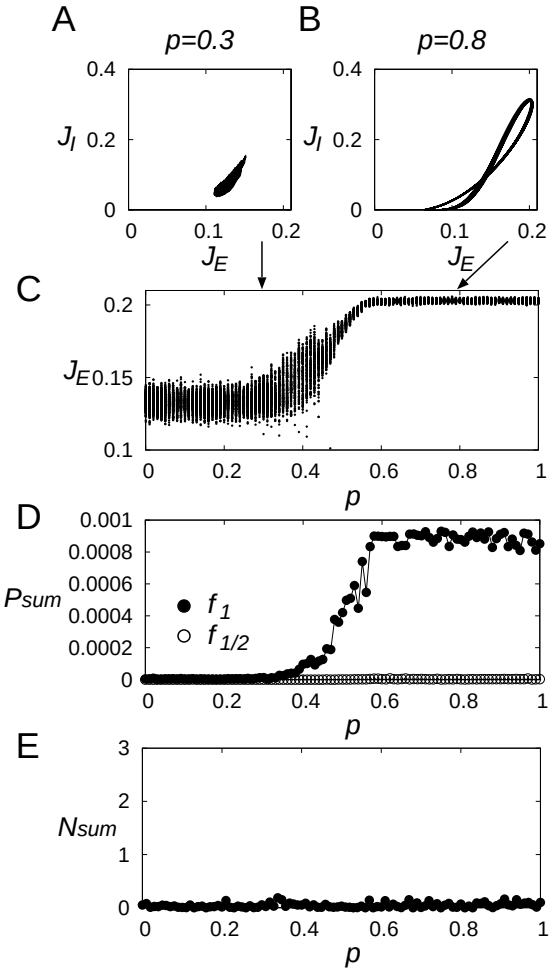

Figure 9: The dependence of the dynamics in the $E\&I$-rewiring network on the rewiring probability p for $g_{ext} = 3.2$. (A), (B) Trajectories on the (J_E, J_I) plane for $p = 0.3$ and $p = 0.8$. (C) Plot of peak values of J_E. (D) The dependence of the sum of powers around f_1 and $f_{1/2}$ on p. (E) Dependence of the sum of nonlinearity on p.

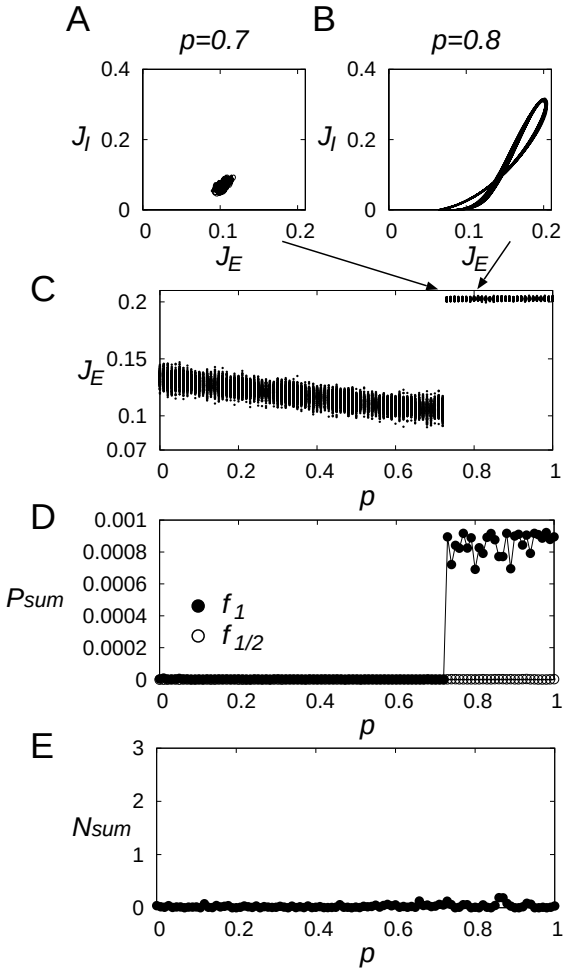

Figure 10: The dependence of the dynamics in the E-rewiring network on the rewiring probability p for $g_{ext} = 3.2$. (A), (B) Trajectories on the (J_E, J_I) plane for $p = 0.7$ and $p = 0.84$. (C) Plot of peak values of J_E. (D) The dependence of the sum of powers around f_1 and $f_{1/2}$ on p. (E) Dependence of the sum of nonlinearity on p.

mined both by the rewired network structure and by the connection strength g_{ext}.

6 Discussion and conclusions

The dependence of the dynamics of pulse-coupled neural networks composed of both excitatory and inhibitory neurons on random rewiring of connections was examined. The network in which both excitatory and inhibitory connections are rewired is called the $E\&I$-rewiring network, while the network in which only excitatory connections are rewired is called the E-rewiring network. In the $E\&I$-rewiring network, when the rewiring probability p is increased from 0, a Hopf-like bifurcation takes place and periodic synchronous firing appears. When p is increased further, a period-doubling bifurcation and chaotic synchronization are observed. In the E-rewiring network, when p is increased from 0, a saddle-node-like bifurcation and chaotic synchronization are observed. When a different value of the connection strength was used, chaos does not necessarily appear, and, in such cases, only periodic synchronization appears. It is because that both the rewiring probability and the connection strength act as bifurcation parameters in our network. These results are observed in the network in which each neuron has both the long-range and short-range connections. We have confirmed that the similar results are also observed in the network in which each neuron has either long-range or short range connections (Buzsáki et al., 2004) (data not shown). Therefore, the observed phenomenon would be robust against the change of the network structure.

To detect the chaotic structure in the network, we used the inter-synchronization intervals of the ensemble-

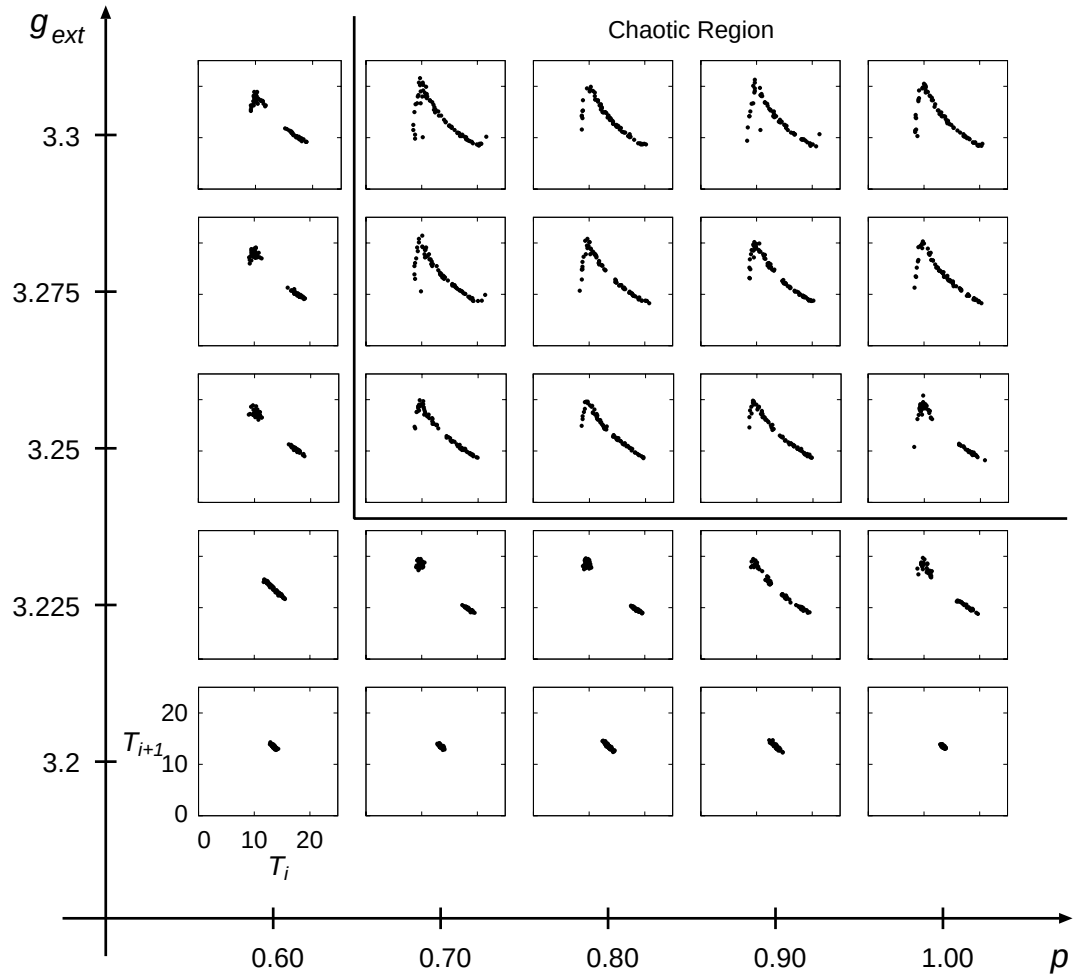

Figure 11: The dependence of the chaotic structure on p and g_{ext}. Each inset shows the return plot (T_i, T_{i+1}) of the ISI. It is observed that chaos (or unimodal structure) exists when both p and g_{ext} are large.

averaged instantaneous firing rate, and the nonlinear prediction method based on reconstruction. Particularly, the sum of nonlinearity defined using the difference between the prediction error of the original data and that of the AAFT surrogate data successfully took large values when low-dimensional unimodal structure of chaos exists in the system. The ensemble-averaged statistics that reflect dynamics of an assembly of neurons such as the field potential are often used in experimental studies; therefore, our method might give a simple method to detect hidden structure of chaos in high-dimensional neural networks. Recently, in experimental studies, irregular firing of single neurons (Softky & Koch, 1993; Shadlen & Newsome, 1994), spontaneous fluctuation between up state and down state of the neural population activity (MacLean et al., 2005; Hoffman et al., 2007; Poulet & Petersen, 2008), and dynamical state-changes in cortical networks (Kenet et al., 2003) were found. Although the mechanisms of such dynamics have not been fully understood, it would be interesting to perform nonlinear analysis of chaos for such experimental data in real neurons and neural networks.

In this paper, chaos emerged when connections of the network are rewired. This phenomenon would be important because the network topologies are attracting considerable attention in neuroscience because they relate to effective transmission of information in the brain (Buzsáki, 2006). It is also noticeable that similar configurations of connections might be realized by regulating connection strengths in the network according to some learning rules, such as Hebbian rule, STDP (Bi & Poo, 2001), short-term synaptic plasticity with facilitation and depression (Markram et al., 1998; Wang et al., 2006), synaptic modulation by acetylcholine (Salgado et al., 2007; Kruglikov et al., 2008), and so on. In other words, the well-known advantages of chaos such as escape from local minima in optimization problems and chaotic transitions among memory states in associative memory models (Aihara et al., 1990; Inoue & Nagayoshi, 1991; Nara & Davis, 1992; Tsuda, 1992; Adachi & Aihara, 1997; Uchiyama & Fujisaka, 2004; Kanamaru, 2007) might be realized as a result of such synaptic plasticity and learning in neural networks.

In our network, there are two kinds of randomness,

namely, noise added to each neuron and random rewiring of connections. Both act as bifurcation parameters to yield chaotic synchronization, in which each neuron fluctuates because of noise, but the ensemble-averaged dynamics can show deterministic chaos. This result suggests that rewiring-induced randomness in the system does not necessarily contaminate the system, and sometimes it even introduces rich dynamics to the system such as chaos. It has already been known that the rewiring can induce periodic or chaotic synchronization in some networks (Barahona & Pecora, 2002; Hong, Choi, & Kim, 2002; Hagberg & Schult, 2008), but the periodic or chaotic dynamics in such networks were determined mainly by the dynamics of each element. In our model, chaos is a property of the rewired network because each neuron has a stable equilibrium and shows neither periodic nor chaotic oscillation when it is disconnected from the other neurons.

Recently, it was reported that the existence of noise can generate chaos in some nonlinear systems with multiple elements (Kanamaru & Sekine, 2005b; Kanamaru, 2006, 2007; Ichiki, Ito, & Shiino, 2007; Kanamaru & Aihara, 2008). In such systems, the behavior of each element is noisy, but by averaging the dynamics of many elements, chaos can emerge. Similarly, it is known that chaos also emerges by introducing variability to some nonlinear systems such as cutting the connections in an associative network (Nara & Davis, 1992), co-evolution of phases and connection weights in coupled phase oscillators (Aoki & Aoyagi, 2009), and so on. The rewiring-induced chaos observed in the present paper would give a new possible scenario to generate chaos in neural systems.

Acknowledgement

This research is partially supported by a Grant-in-Aid for Encouragement of Young Scientists (B) (No. 20700215), a Grant-in-Aid for Scientific Research on Priority Areas -System study on higher-order brain functions- from the Ministry of Education, Culture, Sports, Science and Technology of Japan (No. 17022012), and the Japan Society for the Promotion of Science (JSPS) through its "Funding Program for World-Leading Innovative R&D on Science and Technology (FIRST Program)."

A Definition of the Network

A pulse-coupled neural network composed of excitatory and inhibitory neurons arranged in a two-dimensional array is considered. An excitatory neuron and an inhibitory neuron are placed at the point (i,j) ($1 \le i \le N_x$, $1 \le j \le N_y$) in the array, and both the number of neurons in the excitatory ensemble and that in the inhibitory ensemble are $N_x N_y$. The dynamics of the internal states $\theta_E^{(i,j)}$ of the excitatory neuron as well as $\theta_I^{(i,j)}$ of the inhibitory neuron at (i,j), is written as

$$\begin{aligned}\tau_X \dot{\theta_X^{(i,j)}} &= (1-\cos\theta_X^{(i,j)}) + (1+\cos\theta_X^{(i,j)}) \\ &\quad \times (r_X + \xi_X^{(i,j)}(t) + g_{XE} I_{XE}^{(i,j)}(t) - g_{XI} I_{XI}^{(i,j)}(t) \\ &\quad + g_{gap}\delta_{XI} I_{gap}^{(i,j)}(t)), \qquad \text{(A.1)}\end{aligned}$$

$$\begin{aligned}I_{XY}^{(i,j)}(t) &= \frac{1}{2\#A_{cXY}^{(i,j)}} \sum_{(m,n)\in A_{cXY}^{(i,j)}} \sum_l \\ &\quad \frac{1}{\kappa_Y} \exp\left(-\frac{t-t_l^{(m,n)}}{\kappa_Y}\right), \qquad \text{(A.2)}\end{aligned}$$

$$\begin{aligned}I_{gap}^{(i,j)}(t) &= \frac{1}{\#A_g^{(i,j)}} \sum_{(m,n)\in A_g^{(i,j)}} \\ &\quad \sin\left(\theta_I^{(m,n)}(t) - \theta_I^{(i,j)}(t)\right), \qquad \text{(A.3)}\end{aligned}$$

$$\langle \xi_X^{(i,j)}(t) \xi_Y^{(m,n)}(t') \rangle = D\delta_{XY}\delta_{im}\delta_{jn}\delta(t-t'), \qquad \text{(A.4)}$$

where $X = E$ or I, and δ_{ij} is Kronecker's delta (Ermentrout, 1996; Izhikevich, 1999; Kanamaru & Aihara, 2008). Each neuron is modeled by the theta neuron (Ermentrout, 1996), which is known as a general model of type-I neuron (Izhikevich, 1999); therefore, the dynamics of our network would also be observed in networks of other type-I neurons. Although the number of excitatory neurons in the cortex is much larger than that of inhibitory neurons, we set both the numbers to be identical for simplicity. As shown in equations A.2 and A.3, the synaptic weights are divided by the number of connected neurons; therefore, the dynamics of the network does not depend on the number of neurons if there is a sufficiently large number of neurons. Connections through chemical synapses are modeled by the postsynaptic potential with an exponential function, and electrical synapses with gap junctions based on physiological observations (Galarreta & Hestrin, 2001) are introduced to the connections between the inhibitory neurons. Electrical synapses correspond to the diffusive coupling in physical systems; therefore, synchronization in the neural system can be induced (Ermentrout, 2006). $I_{XY}^{(i,j)}$ denotes the inputs by chemical synapses from the ensemble Y to the neuron at (i,j) in the ensemble X. $A_{cXY}^{(i,j)}$ denotes a set of indices at which there is a neuron in the ensemble Y, which connects to the neuron at (i,j) in the ensemble X. $\#A_{cXY}^{(i,j)}$ is the number of elements of this set. $t_l^{(m,n)}$ denotes the lth firing time of the neuron at (m,n) in the ensemble Y and is defined by the time at which $\theta_Y^{(m,n)}$ exceeds π. $I_{gap}^{(i,j)}(t)$ is the input by electrical synapses. $A_g^{(i,j)}$ denotes the set of indices at which there is a neuron that connects to the target neuron through electrical synapses. r_X denotes the parameters of the neurons in ensemble X. Without Gaussian white noise $\xi_X^{(i,j)}(t)$ and input $I_{XY}^{(i,j)}$, a single neuron shows self-oscillation when $r_X > 0$. When $r_X < 0$, on the other hand, this neuron becomes an excitable system with the following stable

equilibrium:

$$\theta_0 = -\arccos\frac{1+r_X}{1-r_X}, \tag{A.5}$$

where θ_0 approaches zero when $r_X \to 0$. In the literature of synchronization in neural systems, many authors examined the synchronization of excitatory oscillators (Mirollo & Strogatz, 1990; Kuramoto, 1991; Abbott & van Vreeswijk, 1993; Tsodyks, Mitkov, & Sompolinsky, 1993; Hansel, Mato, & Meunier, 1995; van Vreeswijk, 1996; Sato & Shiino, 2002) or inhibitory oscillators (van Vreeswijk, Abbott, & Ermentrout, 1994; Wang & Buzsáki, 1996; White et al., 1998; Golomb & Hansel, 2000; Lewis & Rinzel, 2003; Nomura, Fukai, & Aoyagi, 2003). However, in the present study, we set $r_E = r_I = -0.025$, and we consider the dynamics of networks composed of excitable neurons only. Our neuron model stays on the stable equilibrium when the noise intensity D is set to zero, irrespective of the values of the connections strength g_{XY} and g_{gap} because there is no firing. When $D > 0$ and $g_{XY} = g_{gap} = 0$, each neuron in our network shows stochastic firing, which is neither periodic nor chaotic. When $D > 0$, $g_{XY} \neq 0$, and $g_{gap} \neq 0$, the firing of neurons in our network is typically asynchronous. However, when the values of D, g_{XY}, and g_{gap} are appropriately chosen and when the network is sufficiently rewired as explained below, synchronous firing appears.

For simplicity, the parameters are set as $g_{EE} = g_{II} \equiv g_{int}$ and $g_{EI} = g_{IE} \equiv g_{ext}$. The time constants of the internal dynamics and the synaptic transmission are set to $\tau_E = 1$, $\tau_I = 0.5$, $\kappa_E = 1$, and $\kappa_I = 5$.

B Algorithm to obtain $A^{(i,j)}(p,k)$

In this section, the algorithm to obtain the rewired connection $A^{(i,j)}(p,k)$ from the local connections $A^{(i,j)}(0,k)$ is explained. From $N\#A^{(i,j)}(0,k)$ connections in the network of N neurons, $Np\#A^{(i,j)}(0,k)$ connections are selected randomly ($N = N_E = N_I$). Let us assume that the connection from the neuron at (s,t) to that at (i,j) is selected, i.e., $(s,t) \in A^{(i,j)}(0,k)$. After selecting a new neuron at (u,v) that is not included in $A^{(i,j)}(0,k)$ randomly, (s,t) is removed from $A^{(i,j)}(0,k)$ and (u,v) is added to $A^{(i,j)}(0,k)$. Then, in order to keep the symmetric connections, (i,j) is removed from $A^{(s,t)}(0,k)$ and added to $A^{(u,v)}(0,k)$. With this procedure, a set $A^{(i,j)}(p,k)$ of rewired connections to the neuron at (i,j) is obtained.

C Definition of $L(p)$ and $C(p)$

In this section we define the average shortest path length $L(p)$ and the clustering coefficient $C(p)$.

The shortest path length between two neurons is the minimum number of synapses to pass for one neuron to reach to another one, and by averaging it over the network, $L(p)$ is obtained.

Next, to define $C(p)$, we define the local clustering coefficient $C_i(p)$. We count the number e_i of pairs of inter-connected neurons which also are connected to the ith neuron. Using the number k_i of neurons that connect to the ith neuron, $C_i(p)$ is defined as

$$C_i(p) = \frac{2e_i}{k_i(k_i-1)}. \tag{C.1}$$

By averaging $C_i(p)$ over all the neurons, $C(p)$ is obtained.

D Nonlinear prediction based on reconstruction

In this section, the nonlinear prediction method based on reconstruction of dynamics is summarized (Theiler et al., 1992; Sauer, 1994; Suzuki, et al., 2000; Shinohara et al., 2002; Kanamaru & Sekine, 2005a; Hirata et al., 2008). With the kth peak time t_k of the firing rate of an excitatory ensemble, the inter-synchronization interval (ISI) is defined as

$$T_k = t_{k+1} - t_k. \tag{D.1}$$

Let us consider an ISI sequence $\{T_k\}$ and the delay coordinate vectors $V_j = (T_{j-m+1}, T_{j-m+2}, \ldots, T_j)$ with the reconstruction dimension m, and let L be the number of vectors in the reconstructed phase space $\boldsymbol{R}^m$. For a fixed integer j_0, we choose $l = \beta L$ ($\beta < 1$) points that are nearest to the point V_{j_0} and denote them by $V_{j_k} = (T_{j_k-m+1}, T_{j_k-m+2}, \ldots, T_{j_k})(k = 1, 2, \ldots, l)$. With $\{V_{j_k}\}$, a predictor of T_{j_0} for h steps ahead is defined as

$$p_{j_0}(h) = \frac{1}{l}\sum_{k=1}^{l} T_{j_k+h}. \tag{D.2}$$

With $p_{j_0}(h)$, the normalized prediction error (NPE) is defined as

$$E_{NP}(h) = \frac{\langle (p_{j_0}(h) - T_{j_0+h})^2 \rangle^{1/2}}{\langle (\langle T_{j_0} \rangle - T_{j_0+h})^2 \rangle^{1/2}}, \tag{D.3}$$

where $\langle \cdot \rangle$ denotes the average over j_0. When the embedded vector V_j has structure such as a strange attractor, we say that the system has deterministic structure. Note that a periodic solution where the firing rate of the network oscillates with an average interval T is regarded as a stochastic process around T; hence it does not have deterministic structure. A small value of NPE *i.e.*, less than 1, implies that the ISI sequence has deterministic structure behind the time series because this algorithm is based on the assumption that the dynamical structure of a finite-dimensional deterministic system can be well reconstructed by the delay coordinates of ISI (Sauer, 1994). However, stochastic time series with large auto-correlations can also take NPE values less than 1. Therefore, we could not conclude that there is deterministic structure only from the magnitude of NPE.

To confirm the deterministic structure, the values of NPE should be compared with those of NPE for a set of surrogate data (Theiler et al., 1992). The surrogate data are new time series generated from the original time series under some null hypotheses so that the new time series preserve some statistical properties of the original data. In the present study we use two kinds of surrogates, namely, random shuffled (RS) and amplitude adjusted Fourier transformed (AAFT) surrogate data which correspond to the null hypothesis of an independent and identically distributed random process and that of a linear stochastic process observed through a monotonic nonlinear function, respectively. To make AAFT surrogate data, we used TISEAN 3.0.1 (Hegger, Kantz, & Schreiber, 1999; Schreiber & Schmitz, 2000). If the values of NPE for the original data are significantly smaller than those of NPE for the surrogate data, the null hypothesis is rejected, and it can be concluded that there is some possibility that the original time series has deterministic structure.

References

Abbott, L. F., & van Vreeswijk, C. (1993). Asynchronous states in networks of pulse-coupled oscillators. *Phys. Rev. E*, 48, 1483–1490.

Adachi, M., & Aihara, K. (1997). Associative dynamics in a chaotic neural network. *Neural Networks*, 10, 83–98.

Aihara, K., Matsumoto, G., & Ikegaya, Y. (1984). Periodic and non-periodic responses of a periodically forced Hodgkin-Huxley oscillator, *J. Theor. Biol.*, 109, 249–269.

Aihara, K., Numajiri, T., Matsumoto, G., & Kotani, M. (1986). Structures of attractors in periodically forced neural oscillators. *Phys. Lett. A*, 116, 313–317.

Aihara, K., Takabe, T., & Toyoda, M. (1990). Chaotic neural networks. *Physics Letters A*, 144, 333–340.

Aihara, K., & Tokuda, I. (2002). Possible neural coding with interevent intervals of synchronous firing. *Phys. Rev. E*, 66, 026212.

Aoki, T., & Aoyagi, T. (2009). Co-evolution of phases and connection strengths in a network of phase oscillators. *Phys. Rev. Lett.*, 102, 034101.

Barahona, M., & Pecora, L. M. (2002). Synchronization in small-world systems. *Phys. Rev. Lett.*, 89, 054101.

Bi, G. & Poo, M. (2001). Synaptic modification by correlated activity: Hebb's postulate revisited. *Annu. Rev. Neurosci.* 24, 139–166.

Brunel, N. (2000). Dynamics of sparsely connected networks of excitatory and inhibitory spiking neurons. *J. Comput. Neurosci.*, 8, 183–208.

Buzsáki, G. (2006). *Rhythms of the brain.* New York: Oxford University Press.

Buzsáki, G., Geisler, C., Henze, D. A., & Wang, X.-J. (2004). Interneuron diversity series: Circuit complexity and axon wiring economy of cortical interneurons. *Trends Neurosci.*, 27, 186–193.

Ermentrout, B. (1996). Type I membranes, phase resetting curves, and synchrony. *Neural Comput.*, 8, 979–1001.

Ermentrout, B. (2006). Gap junctions destroy persistent states in excitatory networks. *Phys. Rev. E*, 74, 031918.

Feudel, U., Neiman, A., Pei, X., Wojtenek, W., Braun, H., Huber, M., & Moss, F. (2000). Homoclinic bifurcation in a Hodgkin-Huxley model of thermally sensitive neurons. *Chaos*, 10, 231–239.

Freeman, W. J. (1987). Simulation of chaotic EEG patterns with a dynamic model of the olfactory system. *Biol. Cybern.* 56, 139–150.

Galarreta, M., & Hestrin, S. (2001). Electrical synapses between GABA-releasing interneurons. *Nature Rev. Neurosci.*, 2, 425–433.

Golomb, D., & Hansel, D. (2000). The number of synaptic inputs and the synchrony of large, sparse neuronal networks, *Neural Comput.*, 12, 1095–1139.

Hagberg, A., & Schult, D. A. (2008). Rewiring networks for synchronization. *Chaos*, 18, 037105.

Hansel, D., Mato, G., & Meunier, C. (1995). Synchrony in excitatory neural networks. *Neural Comput.*, 7, 307–337.

Hayashi, H., Ishizuka, S., Ohta, M., & Hirakawa, K. (1982). Chaotic behavior in the onchidium giant neuron under sinusoidal stimulation. *Phys. Lett.*, 88A, 435–438.

Hegger, R., Kantz, H., & Schreiber, T. (1999). Practical implementation of nonlinear time series

methods: The TISEAN package. *Chaos*, 9, 413–435.

Hirata, Y., Katori, Y., Shimokawa, H., Suzuki, H., Blenkinsop, T.A., Lang, E.J., Aihara, K. (2008). Testing a neural coding hypothesis using surrogate data. *Journal of Neuroscience Methods*, 172, 312–322.

Hoffman, K.L., Battaglia, F.P., Harris, K., MacLean, J.N., Marshall, L., & Mehta, M.R. (2007). The upshot of Up states in the neocortex: From slow oscillations to memory formation. *J. Neurosci.*, 27, 11838–11841.

Hong, H., Choi, M. Y., & Kim, B. J. (2002). Synchronization on small-world networks. *Phys. Rev. E*, 65, 026139.

Ichiki, A., Ito, H., & Shiino, M. (2007). Chaos-nonchaos phase transitions induced by multiplicative noise in ensembles of coupled two-dimensional oscillators. *Physica E*, 40, 402–405.

Inoue, M., & Nagayoshi, A. (1991). A chaos neuro-computer. *Physics Letters A*, 158, 373–376.

Izhikevich, E. M. (1999). Class 1 neural excitability, conventional synapses, weakly connected networks, and mathematical foundations of pulse-coupled models. *IEEE Trans. Neural Networks*, 10, 499–507.

Kanamaru, T. (2006). Blowout bifurcation and on-off intermittency in pulse neural networks with multiple modules. *International Journal of Bifurcation and Chaos*, 16, 3309–3321.

Kanamaru, T. (2007). Chaotic pattern transitions in pulse neural networks. *Neural Networks*, 20, 781–790.

Kanamaru, T., & Aihara, K. (2008). Stochastic synchrony of chaos in a pulse-coupled neural network with both chemical and electrical synapses among inhibitory neurons. *Neural Comput.*, 20, 1951–1972.

Kanamaru, T., & Aihara, K. (2010). Roles of inhibitory neurons in rewiring-induced synchronization in pulse-coupled neural networks. *Neural Comput.*, 22, 1383–1398.

Kanamaru, T., & Sekine, M. (2005a). Detecting chaotic structures in noisy pulse trains based on interspike interval reconstruction. *Biol. Cybern.*, 92, 333–338.

Kanamaru, T., & Sekine, M. (2005b). Synchronized firings in the networks of class 1 excitable neurons with excitatory and inhibitory connections and their dependences on the forms of interactions. *Neural Comput.*, 17, 1315–1338.

Kenet, T., Bibitchkov, D., Tsodyks, M., Grinvald, A., & Arieli, A. (2003). Spontaneously emerging cortical representations of visual attributes, *Nature* **425**, 954–956.

Kitano, K., & Fukai, T. (2007). Variability v.s. synchronicity of neuronal activity in local cortical network models with different wiring topologies. *J. Comput. Neurosci.*, 23, 237–250.

Kruglikov, I. & Rudy, B. (2008). Perisomatic GABA release and thalamocortical integration onto neocortical excitatory cells are regulated by neuromodulators. *Neuron*, 58, 911–924.

Kuramoto, Y. (1991). Collective synchronization of pulse-coupled oscillators and excitable units. *Physica D*, 50, 15–30.

Lago-Fernández, L. F., Huerta, R., Corbacho, F., & Sigüenza, J. A. (2000). Fast response and temporal coherent oscillations in small-world networks. *Phys. Rev. Lett.*, 84, 2758–2761.

Lewis, T. J., & Rinzel, J. (2003). Dynamics of spiking neurons connected by both inhibitory and electrical coupling. *J. Comput. Neurosci.*, 14, 283–309.

MacLean, J.N., Watson, B.O., Aaron, G.B., & Yuste, R. (2005). Internal dynamics determine the cortical response to thalamic stimulation. *Neuron*, 48, 811–823.

Markram, H., Wang, Y., & Tsodyks, M. (1998). Differential signaling via the same axon of neocortical pyramidal neurons. *Proc. Natl. Acad. Sci. USA*, 95, 5323–5328.

Masuda, N., & Aihara, K. (2004). Global and local synchrony of coupled neurons in small-world networks. *Biol. Cybern.*, 90, 302–309.

Matsumoto, G., Aihara, K., Ichikawa, M., & Tasaki, A. (1984). Periodic and nonperiodic responses of membrane potentials in squid giant axons during sinusoidal current stimulation. *J. Theoret. Neurobiol.* 3, 1–14.

Mirollo, R. E., & Strogatz, S. H. (1990). Synchronization of pulse-coupled biological oscillators. *SIAM J. Appl. Math.*, 50, 1645–1662.

Munro, E., & Börgers, C. (2010). Mechanisms of very fast oscillations in networks of axons coupled by gap

junctions. *J. Comput. Neurosci.*, 28, 539–555.

Nara, S., & Davis, P. (1992). Chaotic wandering and search in a cycle-memory neural network. *Progress of Theoretical Physics*, 88, 845–855.

Netoff, T. I., Clewley, R., Arno., S., Keck, T., & White, J. A. (2004). Epilepsy in small-world networks. *J. Neurosci.*, 24, 8075–8083.

Nomura, M., Fukai, T., & Aoyagi, T. (2003). Synchrony of fast-spiking interneurons interconnected by GABAergic and electrical synapses. *Neural Comput.*, 15, 2179–2198.

Ott, E. (1993). *Chaos in Dynamical Systems.* Cambridge University Press, New York.

Poulet, J.F.A., & Petersen, C.C.H. (2008). Internal brain state regulates membrane potential synchrony in barrel cortex of behaving mice. *Nature*, 454, 881–885.

Roxin, A., Riecke, H., & Solla, S. A. (2004). Self-sustained activity in a small-world network of excitable neurons. *Phys. Rev. Lett.*, 92, 198101.

Salgado, H., Bellay, T., Nichols, J.A., Bose, M., Martinolich, L., Perrotti, L., & Atzori, M. (2007). Muscarinic M_2 and M_1 receptors reduce GABA release by Ca^{2+} channel modulation through activation of PI_2K/Ca^{2+}-independent and PLC/Ca^{2+}-dependent PKC. *Journal of Neurophysiology* 98, 952–965.

Sato, Y. D., & Shiino, M. (2002). Spiking neuron models with excitatory or inhibitory synaptic couplings and synchronization phenomena. *Phys. Rev. E*, 66, 041903.

Sauer, T. (1994). Reconstruction of dynamical systems from interspike interval. *Rhys. Rev. Lett*, 72, 3811–3814.

Schreiber, T., & Schmitz, A. (2000). Surrogate time series. *Physica D*, 142, 346–382.

Shadlen, M. N., & Newsome, W.T. (1994). Noise, neural codes and cortical organization. *Curr. Opin. in Neurobiol.*, 4, 569–579.

Shinohara, Y., Kanamaru, T., Suzuki, H., Horita, T., & Aihara, K. (2002). Array-enhanced coherence resonance and forced dynamics in coupled FitzHugh-Nagumo neurons with noise. *Phys. Rev. E*, 65, 051906.

Softky, W.R., & Koch, C. (1993). The highly irregular firing of cortical cells is inconsistent with temporal integration of random EPSPs, *J. Neurosci.*, 13, 334–350.

Strogatz, S. H. (2001). Exploring complex networks. *Nature*, 410, 268–276.

Suzuki, H., Aihara, K., Murakami, J., & Shimozawa, T. (2000). Analysis of neural spike trains with interspike interval reconstruction. *Biol. Cybern.*, 82, 305–311.

Theiler. J., Eubank. S., Longtin. A., Galdrikian. B., & Farmer. J.D. (1992). Testing for nonlinearity in time series: the method for surrogate data. *Physica D*, 58, 77–94.

Traub, R.D., Schmitz, D., Jefferys, J.G.R., & Draguhn, A. (1999). High-frequency population oscillations are predicted to occur in hippocampal pyramidal neuronal networks interconnected by axoaxonal gap junctions. *Neuroscience*, 92, 407–426.

Tsodyks, M., Mitkov, I., & Sompolinsky, H. (1993). Pattern of synchrony in inhomogeneous networks of oscillators with pulse interactions. *Phys. Rev. Lett.*, 71, 1280–1283.

Tsuda, I. (1992). Dynamic link of memory – Chaotic memory map in nonequilibrium neural networks. *Neural Networks*, 5, 313–326.

Tsuda, I., Fujii, H., Tadokoro, S., Yasuoka, T., & Yamaguti Y. (2004). Chaotic itinerancy as a mechanism of irregular changes between synchronization and desynchronization in a neural network. *J. Integr. Neurosci.*, 17, 159.

Uchiyama, S., & Fujisaka, H. (2004). Chaotic itinerancy in the oscillator neural network without Lyapunov functions. *Chaos*, 14, 699–706.

Varona, P., Torres, J. J., Huerta, R., Abarbanel, H. D. I., & Rabinovich, M. I. (2001). Regularization mechanisms of spiking-bursting neurons. *Neural Networks*, 14, 865–875.

van Vreeswijk, C. (1996). Partial synchronization in populations of pulse-coupled oscillators. *Phys. Rev. E*, 54, 5522–5537.

van Vreeswijk, C., Abbott, L. F., & Ermentrout, G. B. (1994). When inhibition not excitation synchronizes neural firing. *J. Comput. Neurosci.*, 1, 313–321.

van Vreeswijk, C., & Sompolinsky, H. (1996). Chaos in neuronal networks with balanced excitatory and

inhibitory activity. *Science*, 274, 1724–1726.

Wang, X.-J., & Buzsáki, G. (1996). Gamma oscillations by synaptic inhibition in a hippocampal interneuronal network. *J. Neurosci.*, 16, 6402–6413.

Wang, Y., Markram, H., Goodman, P.H., Berger, T.K., Ma, J. and Goldman-Rakic, P.S. (2006). Heterogeneity in the pyramidal network of the medial prefrontal cortex. *Nature Neuroscience*, 9, 534–542.

Watts, D. J., & Strogatz, S. H. (1998). Collective dynamics of 'small-world' networks. *Nature*, 393, 440–442.

White, J. A., Chow, C. C., Ritt, J., Soto-Treviño, C., & Kopell, N. (1998). Synchronization and oscillatory dynamics in heterogeneous, mutually inhibited neurons. *J. Comput. Neurosci.*, 5, 5–16.